8. Deformation Behavior of Aluminium Armour Plates Impacted by High Hardness Steel Projectiles

8.1. Introduction

Ballistic impact is highly localized process. Heat generated during such severe and rapid impact may induce local thermal softening and microstructural instability. The research activities in the field of ballistic impact have been mainly focused on experimental tests, understanding the behavior of materials under high strain rate loading and creation of analytical models. However, majority of these investigations to a certain extent lack the inclusion of starting microstructure and its subsequent modifications during projectile impact. It is, therefore, of interest to study the deformation behavior of different aluminium alloys based on microstructural modifications in post impact materials.

The ballistic behavior of 70 mm thick plates of three different series of heat treatable aluminium alloys namely AA 2024, AA 6061 and AA 7017 subjected to the impact of 7.62 mm and 12.7 mm high hardness steel projectiles have been investigated. The changes in the microstructure, hardness and damage pattern in post impact samples with respect to the two different projectiles have been studied. All these will be dealt with in this chapter of the thesis.

8.2. Results

8.2.1. Initial microstructure

The starting microstructures of the different aluminium alloy plates are given in Fig.8.1. The microstructural analysis demonstrates the typical features of heat treatable aluminium alloys consisting of large crystalline grains surrounded by hardening precipitates. All the alloy plates demonstrate unrecrystallised pancake shaped grain structure elongated along the rolling direction.

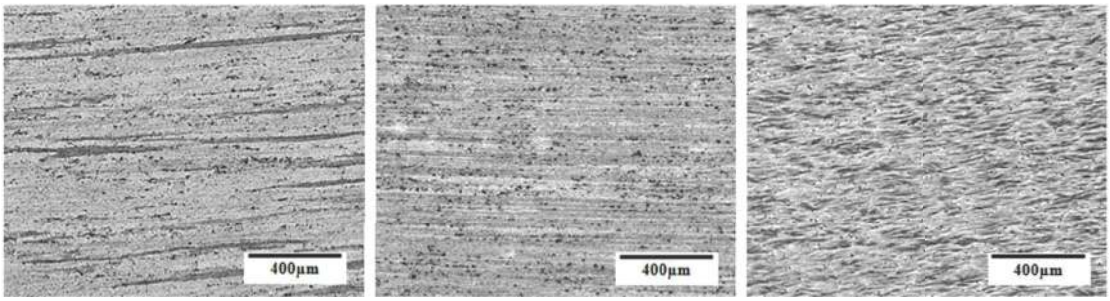

Fig. 8.1: Microstructure of the aluminium alloy plates (a) AA 2024 (b) AA 6061 (c) AA 7017 alloy.

8.2.2. Mechanical Properties

The representative engineering and true stress-strain curve of the three alloys are displayed in Fig.8.2. The σ_{YS}, σ_{UTS}, total elongation, hardness values of these alloys are summarized in Table 8.1. It is evident from Fig 8.2 and Table 8.1 that AA 7017 and AA 6061 plates display the highest and lowest strength (σ_{YS}, σ_{UTS}) values, respectively. The AA 2024 alloy plate exhibits highest value of ductility measured in terms of total elongation to failure followed by the AA 7017 and AA 6061 materials.

Strain hardening behaviors of the three aluminium alloy plates are shown in Fig. 8.3. The material displays two typical slopes in log (true stress) vs. log (true plastic strain) curves. Strain hardening exponents (n) are calculated from the slopes of the curves at lower and

higher strain regimes by using Ludwigson's relation as shown in equation 8.1[Ludwigson, 1971].

$$\sigma = K_1\varepsilon^{n_1} + \exp(K_2 + n_2\varepsilon) \text{---------- (8.1)}$$

Where σ and ε are true plastic stress and true plastic strain while n_1 and n_2 are strain-hardening exponents in higher and lower strain regimes, respectively and K_1, K_2 are constants. The 'n_1 and n_2'values of different alloy plates are shown in Table 8.1. The AA 2024 alloy plate displays the highest strain hardening exponent value in high strain regime followed by AA 6061 and AA 7017 plates.

8.2.3. Ballistic evaluation

The visual comparison of the aluminium alloy plates after ballistic impact against 7.62 mm hard steel projectiles is exhibited in Fig. 8.4. The damage mechanisms displayed by all the three alloy targets clearly indicates that the projectiles has entered into the plates by causing ductile hole enlargement. A close view of the front damage pattern elucidates that the material flows out to form perfect petalling damage pattern in the front side of the AA 2024 and AA 6061 plates. In contrast, broken petal damage is observed in the front face of the AA 7017 plate. All the aluminium alloy plates have successfully stopped the 7.62 mm projectiles. No bulging is observed at the rear face of any of the plates. The aluminium alloy plates after ballistic impact against 12,7mm hard steel projectiles is displayed in Fig. 8.5. It can be seen that all the aluminium alloy plates fail to stop the 12.7 mm projectiles. The projectiles have penetrated through the AA 7017 plates. However, the projectile is seen to remain wedged in the plates. In the same time, a complete perforation is observed in AA 2024 and AA 6061 plates. The variation of ballistic performance of the AA 2024, AA 6061 and AA 7017 plates in terms of DOP against 7.62 mm projectiles is given in Fig. 8.6. This clearly shows that the ballistic penetration resistance of the AA 7017 plate is superior to those of the AA 2024 and AA 6061 plates.

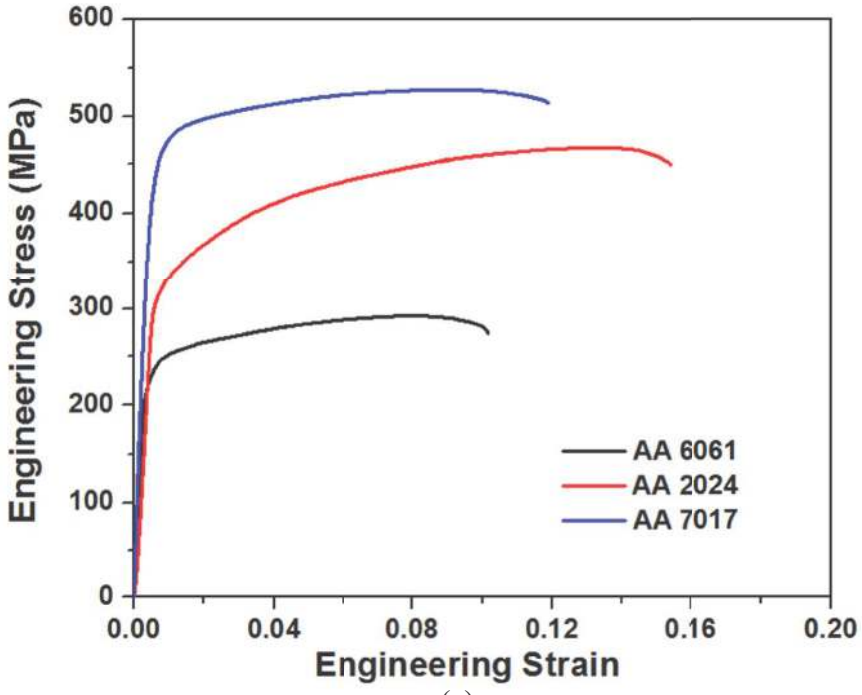

(a)

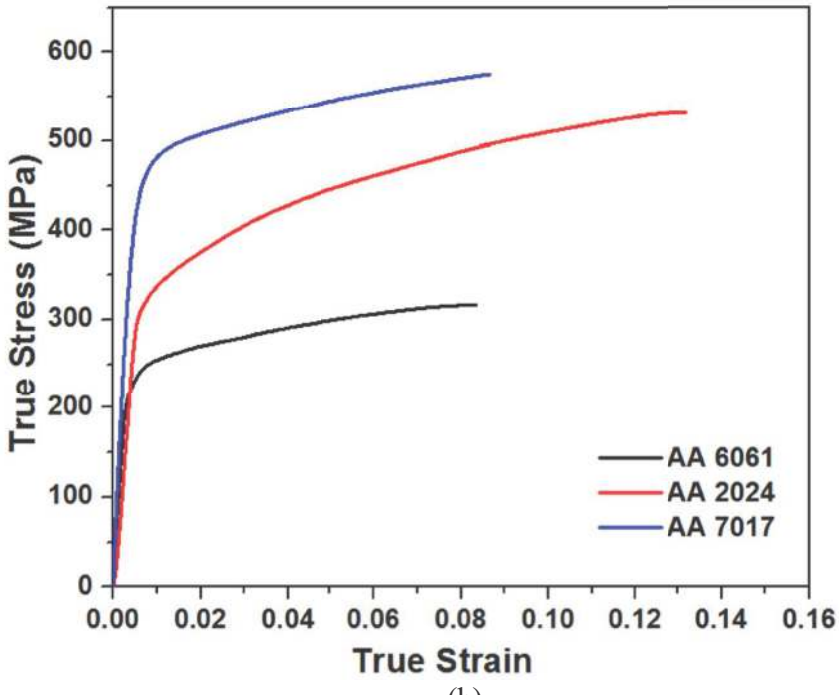

(b)

Fig. 8.2: (a) Engineering stress-strain curves and (b) True stress-strain curves of the three studied aluminium alloys.

Table 8.1: Mechanical properties of the three studied aluminium alloys.

Aluminium Alloy	σ_{YS} MPa	σ_{UTS} MPa	% Elongation	Hardness VHN	n_1	n_2
AA 2024	310	457	16.2	130	0.167	-165.4
AA 6061	250	294	10.4	107	0.113	-191.0
AA 7017	458	513	11.4	160	0.082	-117.0

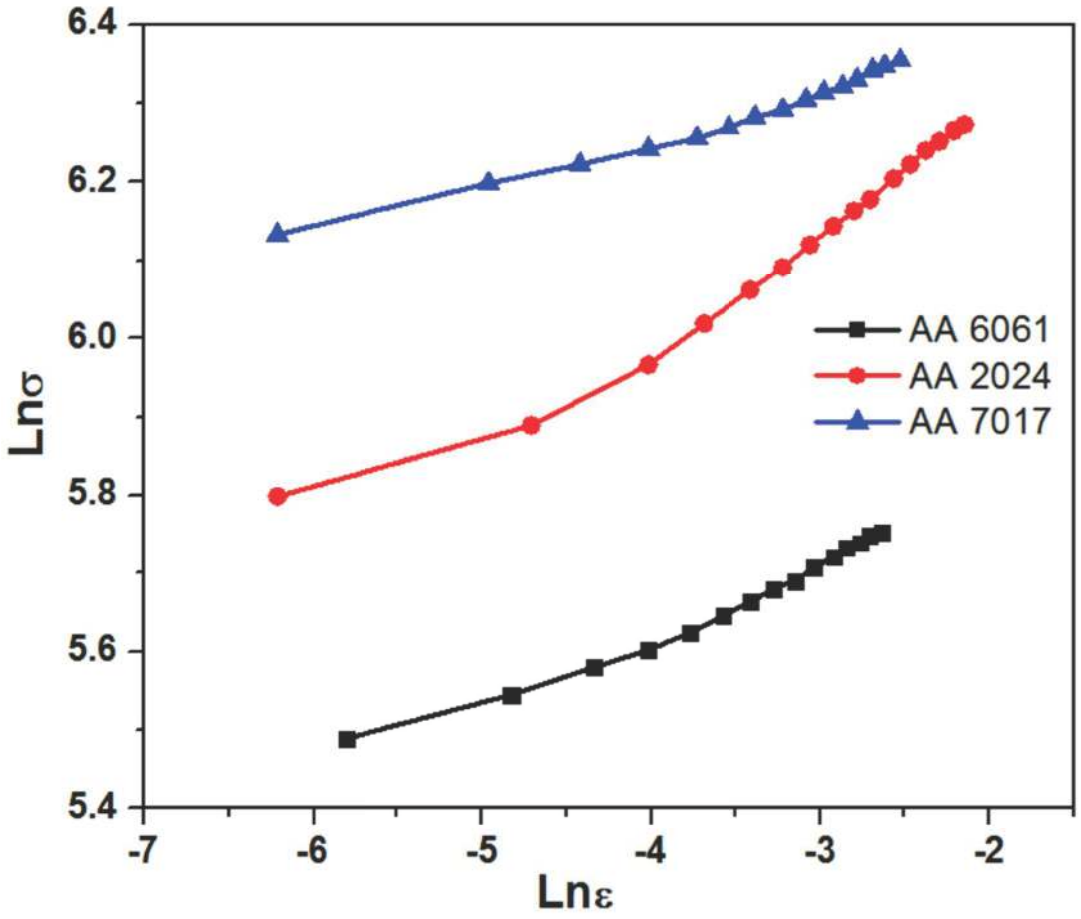

Fig. 8.3: True stress–true plastic strain curves on log scales up to UTS of the three aluminium alloys.

8.2.4. Post ballistic microstructural characterisation

The impact craters of all the three alloys against both types of projectiles are examined in detail to observe the changes in microstructure. The post ballistic microstructures of the AA 2024, AA 6061 and AA 7017 plates impacted with 7.62 mm projectile are shown in Fig. 8.7(a-c). The projectile penetration path can be broadly divided into two regions (A and B) from the prospective of observation of deformed grains (Fig.8.7). In region A, large material deformation is observed along with a few cracks. Severely distorted material flow lines are present in this region. In the region B, material flow lines are smooth and curved in the projectile penetration direction. Adiabatic shear bands (ASBs) are not observed in the microstructure of the craters formed by 7.62 mm projectile. Similar observations are made in the microstructures of craters formed by the impact of 12.7 mm projectiles (Fig 8.8(a-c)). The microstructures of AA 6061 plates display the presence of extensive ASBs throughout the path of the projectile. A few ASBs are also seen in AA 7017 plates. However, no ASBs are observed in the crater region of AA 2024 plates. The inside microstructure of ASBs is seen to be different than the matrix (Fig. 8.8 b).

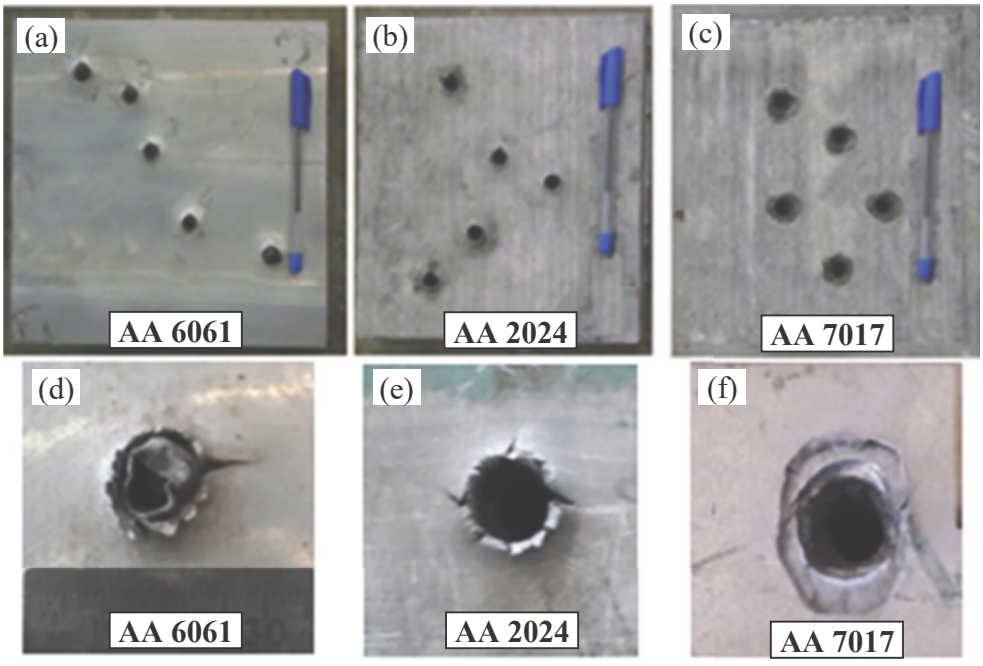

Fig. 8.4: (a) (b) (c) Front face of the aluminium alloy plates after ballistic impact against 7.62 mm projectile; (d),(e),(f) Close up view of the damage patterns.

8.2.5. Post ballistic micro-hardness measurements

Micro-hardness measurements are taken, starting from close to the crater wall and gradually moving away. The variation in micro-hardness values of the AA 2024, AA 6061 and AA 7017 target plates against 7.62 mm and 12.7 mm projectiles are displayed in Fig. 8.9. In AA 2024 impacted plates, there is an initial rise in the hardness value and then it decreases with distance from crater wall till it reaches the base hardness of the plate. For AA 6061 and AA 7017 plates, the hardness starts from a low value and gradually increases. Subsequently the hardness decreases with distance. The extent of rise in hardness is more in 12.7 mm impacted craters than that of the 7.62 mm.

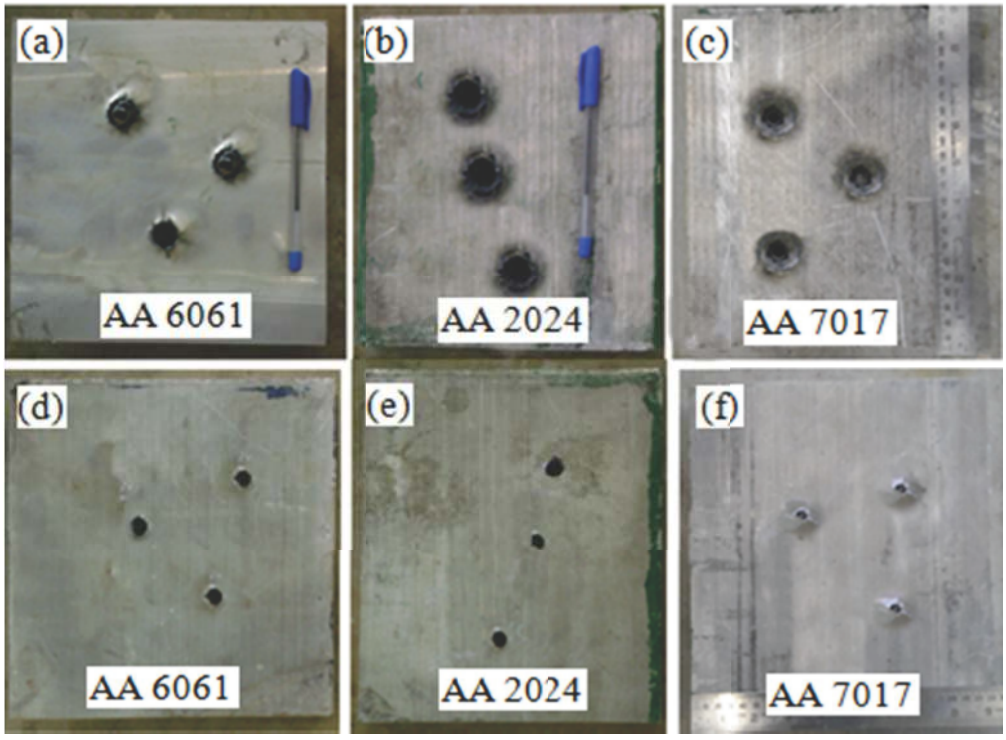

Fig.8.5: (a) (b) (c) Front face of the aluminium alloy plates after ballistic impact against 12.7 mm projectile; (d),(e),(f) Rear face of the aluminium alloy plates after ballistic impact against 12. 7mm projectile.

8.3. Discussion

The alloys AA 2024, AA 6061 and AA 7017 belong to the series of heat treatable aluminium alloys. They acquire their optimum properties through a process of thermal treatment i.e. solution treatment followed by aging. Aging process causes the formation of coherent precipitates leading to high strength and hardness of the material. The effect of thermal treatment process on the microstructure and mechanical properties of AA 2024, AA 6061 and AA 7017 plates has been studied thoroughly. It has been reported that Al_2CuMg, Mg_2Si, $MgZn_2$ precipitates are formed during aging of AA2024, AA6061, and AA7017 plates, respectively [Manes et al., 2014; Borvik et al., 2009; Rout and Ghosh, 2012]. The presence of fine precipitates in the microstructure of the present alloys is also observed (Fig.8.1). The variation in strength and hardness in present aluminium alloys can therefore be attributed to the amount of alloying additions and morphology of the precipitate phases. The AA 7017 plate displays the highest strength and hardness owing to the presence of higher percentage of alloying elements in comparison to those of AA 2024 and AA 6061 plates.

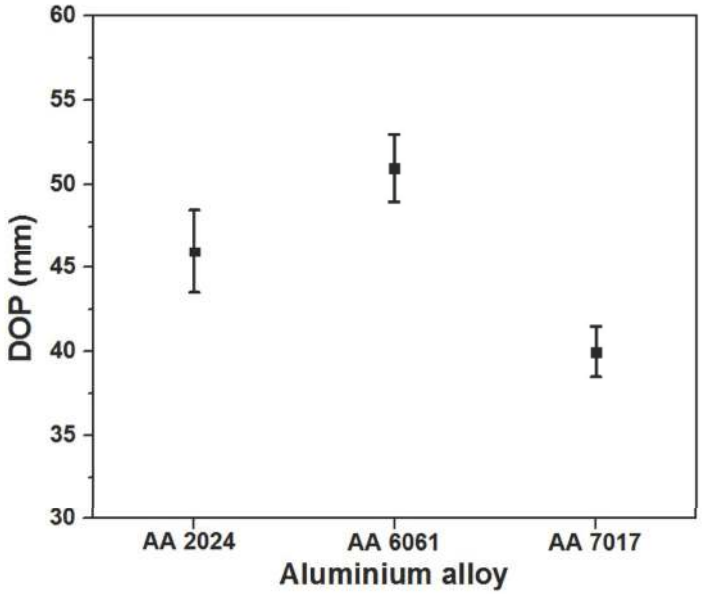

Fig. 8.6: The variation of DOP values of AA 2024, AA 6061, AA 7017 plates against 7.62 mm ammunition.

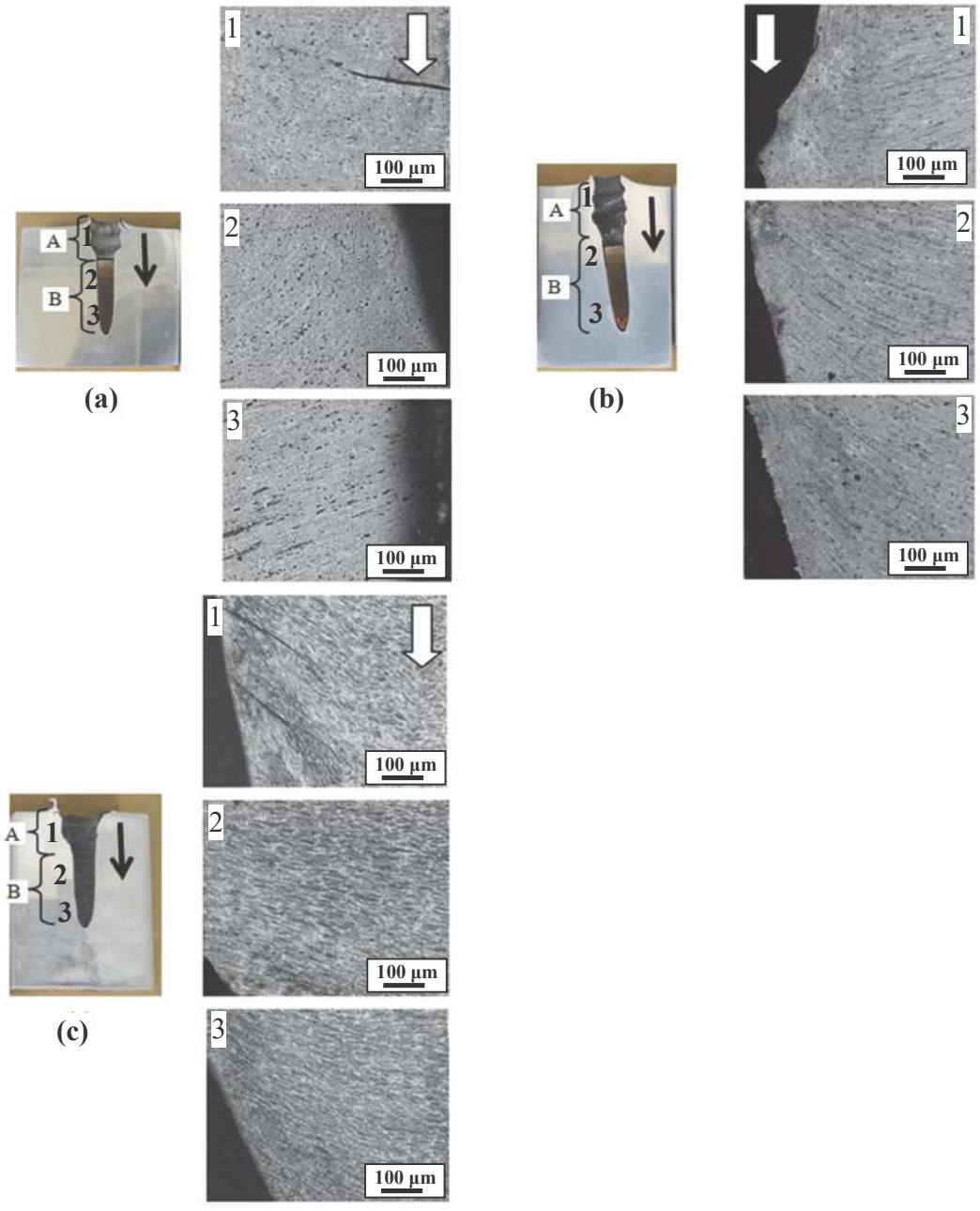

Fig. 8.7: Post ballistic characterisation of the aluminium alloy plates subjected to the impact of 7.62 mm projectile. Micro-structure of (a)AA 2024 (b) AA 6061 (c) AA 7017 plates. Arrow mark indicates the projectile penetration direction. The numbers in the microstructures indicate the corresponding regions of the crater wall.

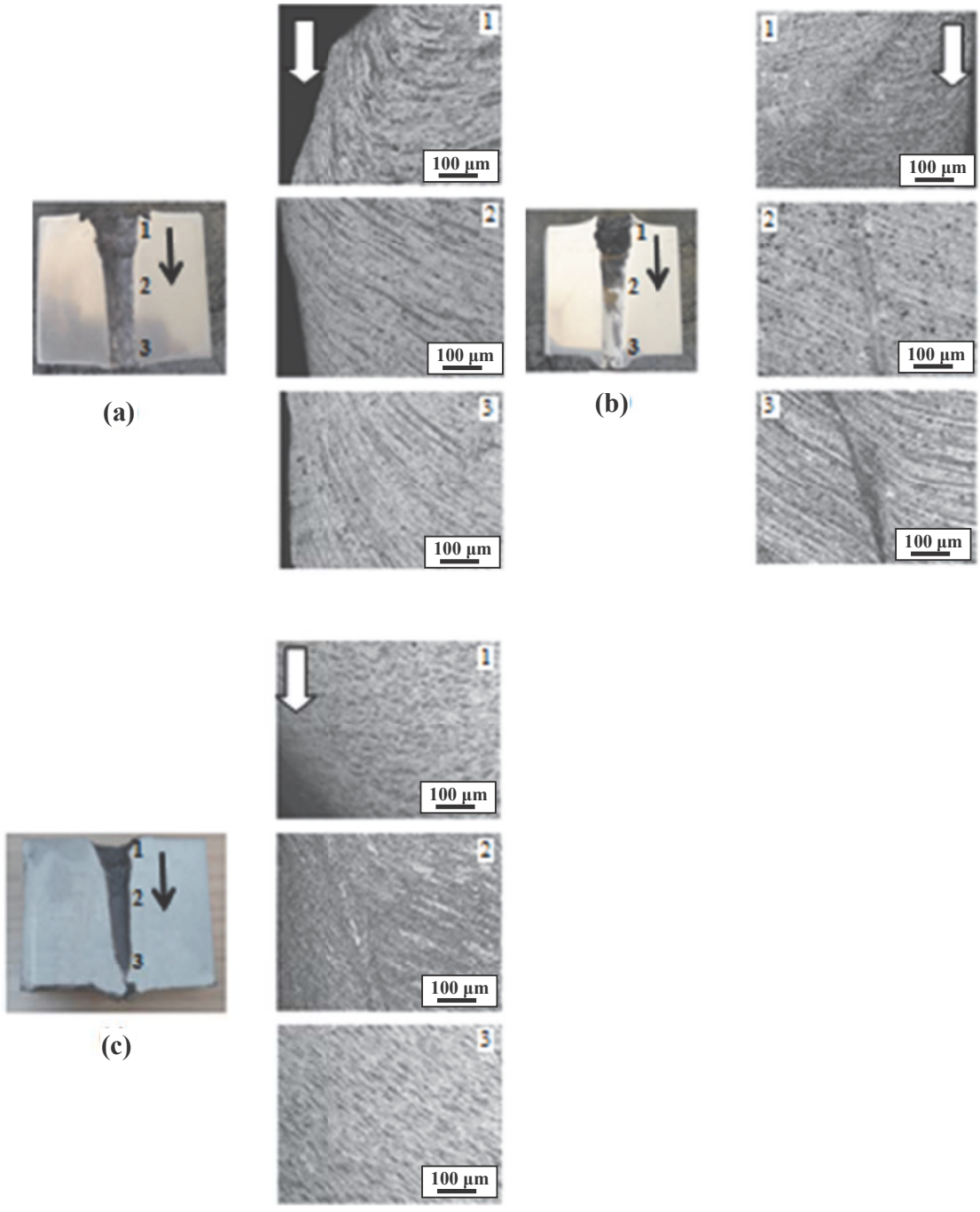

Fig. 8.8: Post ballistic characterisation of the aluminium alloy plates subjected to the impact of 12.7 mm projectile. Micro-structure of (a)AA 2024 (b) AA 6061 (c) AA 7017 plates. Arrow mark indicates the projectile penetration direction. The numbers in the microstructures indicate the corresponding regions of the crater wall.

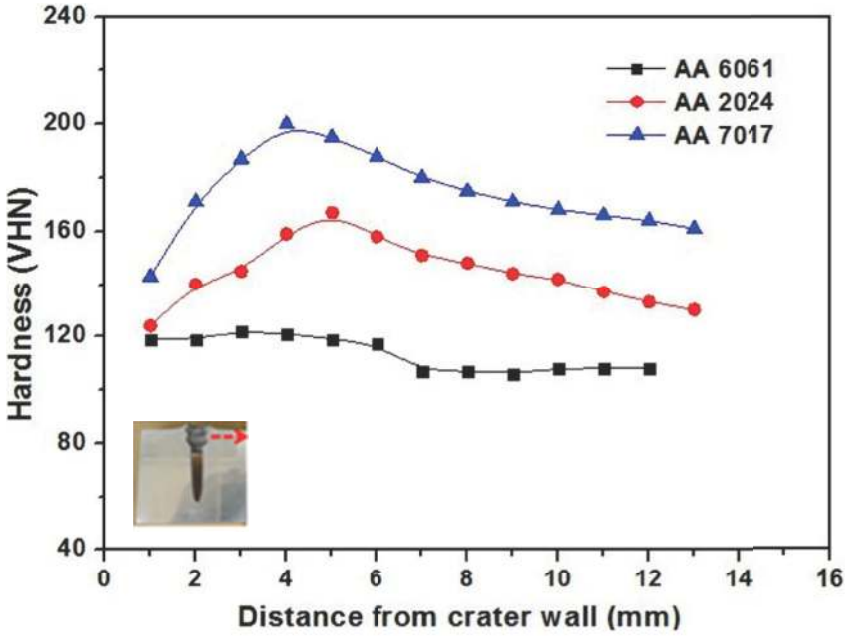

(a)

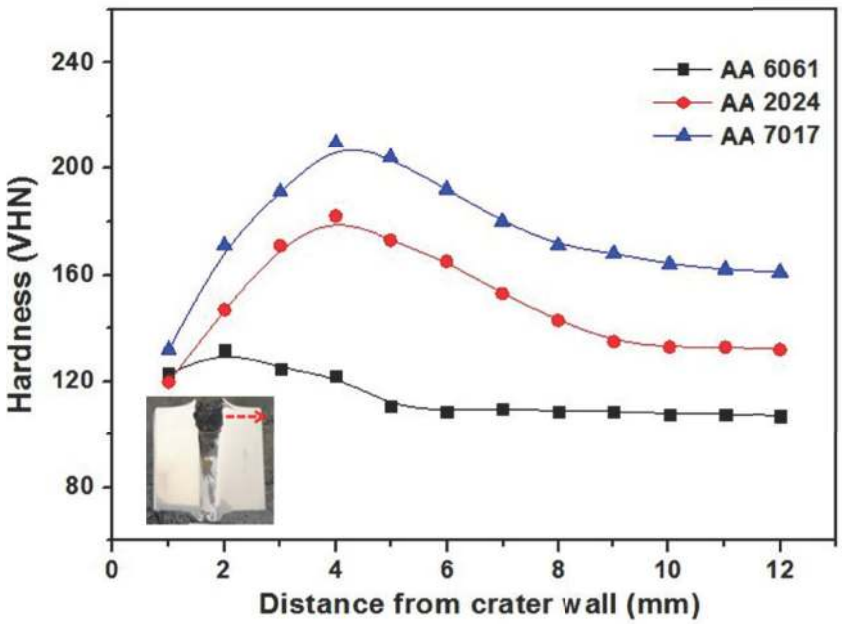

(b)

Fig. 8.9: Micro-hardness measurements of craters impacted by (a) 7.62 mm projectile (b) 12.7 mm projectile

During ballistic impact, the kinetic energy (KE) of the projectile is transmitted to the target plate. The KE of the 7.62 mm and 12.7 mm projectiles are given in Table 2.5. The 12.7 mm projectile carries almost six times higher KE than that of 7.62 mm. It thus, explains the failure of AA2024, AA6061 and AA7017 target plates to stop the 12.7 mm projectiles. The AA 7017 plate displays the best ballistic resistance against both the projectiles in comparison to those of the AA 2024 and AA 6061 plates (Figs. 8.5 and 8.6). This can be ascribed to the higher strength and hardness associated with AA 7017 plates. When projectile impacts on a metallic plate, energy absorption takes place by plastic deformation. As a result, material properties which resist the flow of material improve the ballistic performance. Also, the increase in strength and hardness values of the target material provides resistance to the projectile and thus assists in its erosion and fracture. The ballistic performance therefore improves with increase in strength and hardness of the material. Similar correlations of ballistic properties with strength and hardness have been reported by earlier investigations [Dikshit et al., 1995; Borvik et al. 2010].

The post-ballistic microstructure gives a good indication of the energy absorption in the material during ballistic testing. When projectile strikes, large amount of KE is distributed over a relatively small volume of target material in a very short span of time. This leads to the deformation of material adjacent to the crater wall and formation of ASBs. In fact, the ASBs are produced due to inhomogeneity in deformation of material subjected to loads at very high strain rate. These are formed when the stress, strain and strain rate reaches to a critical condition in which thermal softening suppresses the strain hardening effect during plastic deformation of a material. The ASBs are prominently observed in the 12.7 mm projectile impacted craters of AA 6061 and AA 7017 plates. In contrast, these are absent near crater wall of 12.7 mm projectile impacted AA 2024 plates. This can be correlated with the higher uniform elongation and n_1 values of AA 2024 plate. High strain hardening exponent value prevents localisation of deformation process and thus leads to a uniform deformation. The ASB region undergoes an instantaneous heating and rapid cooling due to their formation in a very short span of time. As a result, the microstructure within the ASBs is different from the matrix.

In the present study ASBs are not observed in the post ballistic microstructure of 7.62 mm projectile impacted target plates. Due to higher thickness of the target plates, a larger volume of the material is involved in the absorption of the impact energy. Thus, the energy dissipated per unit volume of the material is not sufficient to form ASBs in case of plates impacted against 7.62 mm projectiles.

The variation in hardness adjacent to the crater wall is a result of strain hardening caused by high applied strain-rate and simultaneous annealing effect by rise in temperature after projectile impact. In case of AA 6061 and AA 7017 plates, the initial drop in hardness adjacent to the crater wall suggests that the thermal softening effect is dominant mechanism during initial deformation. This is confirmed from the observation of ASBs in the post ballistic microstructure of these two alloy plates. This can be correlated with the low strain hardening exponent values of these two alloy plates. Due to low strain hardening exponent values, the material deforms in a non uniform way. Hence, the heat gets constricted in a narrow region and leads to thermal softening. The behavior of micro-hardness curves for the three alloys is similar against both the projectiles. However, a higher rise in hardness values are observed in case of 12.7 mm projectile impacted craters which can be attributed to higher KE of the 12.7 mm projectile.

8.4. Conclusions

The AA 7017 alloy exhibits the best ballistic performance among the studied materials against both type of high hardness projectiles. Ballistic penetration resistance of the present alloys is in accordance with their strength and hardness values. It appears that the strength and hardness values are more dominant parameters against both the projectiles than the ductility. An apparent difference is observed in the post ballistic microstructures and micro-hardness observations of the alloys. The AA 2024 plate exhibits uniform deformation while an adiabatic mode of failure is detected in AA 6061 and AA 7017 plates. The 12.7 mm projectile has introduced larger material deformation in comparison to 7.62 mm projectile.